ISSN 1063-4576, Journal of Superhard Materials, 2022, Vol. 44, No. 5, pp. 339–349. © Allerton Press, Inc., 2022.
Ukrainian Text © The Author(s), 2022, published in Nadtverdi Materialy, 2022, Vol. 44, No. 5, pp. 48–59.

PRODUCTION, STRUCTURE, PROPERTIES

Structure Formation in Silicon Carbide–Alumina Composites during Electroconsolidation

E. S. Gevorkyan[a], *, V. P. Nerubatskyi[a], R. V. Vovk[b], V. O. Chyshkala[b], and M. V. Kislitsa[b]

[a] *Ukrainian State University of Railway Transport, Kharkiv, 61050 Ukraine*

[b] *Karazin Kharkiv National University, Kharkiv, 61000 Ukraine*

**e-mail: edsgev@gmail.com*

Received January 21, 2022; revised February 4, 2022; accepted February 7, 2022

Abstract—Some possible methods for improving the hot pressing of SiC ceramics are reviewed. The method of liquid-phase sintering is described as a way to increase the physical and mechanical properties and to reduce the energy consumption of the pressing process. An example of liquid-phase sintering of silicon carbide ceramics by the method of hot pressing with use of a direct electric current for the introduction of a small amount of oxide impurities is given. The peculiarities of structure formation and the properties of the composite material based on silicon carbide micropowders, which is obtained by hot pressing in vacuum and heating with a direct high-ampere current transmitted through a graphite mold, are described. The microstructure and the physical and mechanical properties of composites of different compositions have been studied. The optimal composition of the initial mixture and the most optimal sintering temperature are determined. The comparison of the physical and mechanical properties of the obtained composite materials is given.

Keywords: silicon carbide, ceramics, hot pressing, electroconsolidation, liquid-phase sintering, nanopowders

DOI: 10.3103/S1063457622050033

INTRODUCTION

Ceramics based on SiC exhibit substantial mechanical strength at high temperatures, as well as wear resistance, low coefficient of thermal expansion, resistance to oxidation at temperatures up to 1500°C, chemical inertness, biocompatibility, corrosion resistance, resistance to radiation effects, and good hardness and heat conductivity parameters [1, 2]. To obtain products with high mechanical properties at elevated temperatures, it is necessary to create nonporous nanocrystalline materials based on SiC [3, 4]. The properties of nanoceramics can substantially differ from the characteristics of traditional ceramics with micrometer-sized grains, and the behavior of characteristics with an increase in the grain size is individual and depends both on the physical nature of the investigated property and on the physicochemical characteristics of the ceramics used. The synthesis of ceramics based on silicon carbide requires high temperatures. Sintering without impurities at temperatures of 2150–2200°C does not allow one to obtain nonporous products both because of low diffusion coefficients and high volatility of SiC at these temperatures [5, 6].

Despite the existence of a wide range of ceramic materials for various purposes, which are developed on the basis of silicon carbide, the high energy and resource consumption reqired for their production, as well as the growing requirements of scientific and technical progress, force the search for ways to create new types of materials with a high level of physical and mechanical characteristics, but a lower sintering temperature. The use of various nanopowders as modifiers is among the main ways to solve these problems [7]. On the other hand, the use of hot pressing with transmission of a high-amperage current through a graphite mold (electroconsolidation) makes it possible to quickly heat the ceramic mixture, which prevents the growth of grains and activates the sintering process [8, 9].

It was established that the powder consolidation rates are substantially increased compared to the rate of traditional sintering both in the case of electric sintering and in the case of microwave sintering [10, 11]. Moreover, consolidation rates can increase by several orders of magnitude for high-intensity processes with high heating rates. This leads to complete compaction of the powders in a very short time while preserving the nanoscale internal structure. Electroconsolidation (electrosintering) makes it possible to

Table 1. Characteristics of α-Al_2O_3 nanoparticles

Nanopowder	Content
Al_2O_3	99.9 wt %
MgO	1000 ppm
CaO	<200 ppm
K_2O	<200 ppm
Fe_2O_3	<50 ppm
Na_2O, SiO_2	<40 ppm

obtain consolidated ceramic materials, such as Al_2O_3, ZrO_2, TiC, and WC, without impurities and with minimum grain growth in about 10 min [12, 13], while traditional sintering requires several hours and special additives that deteriorate the properties of the material. At the same time, both electrically conductive and nonconductive powders are electroconsolidated with equally high success (using electrically conductive graphite molds) [14], and microwave sintering is successfully used for sintering both the ceramics and metals [15]. This confirms the urgent need for fundamental research on the consolidation of nanostructured bodies activated by an electromagnetic field, primarily through theoretical analysis and model experiments, which are rarely used now in this field of materials science.

EXPERIMENTAL

The submicrometer SiC powder (0.1–0.3 μm) obtained by the method of self-propagating high-temperature synthesis (SHS) [16] was used as a starting material (Fig. 1).

We used ZrO_2 nanopowders partially stabilized with 3 mol % Y_2O_3 (Fig. 2) from the Donetsk Institute of Physics and Engineering, National Academy of Sciences of Ukraine, and α-Al_2O_3 nanopowders with a grain size of 30–50 nm (Fig. 3) from the NANOE Company (France). The characteristics of α-Al_2O_3 nanoparticles are given in Table 1.

A unique Activator 2S high-energy mill was used for the preparation of powder mixtures. The energy saturation of the grinding process was 3 W/h.

The microstructure was studied by scanning electron microscopy [17, 18]. The X-ray diffraction spectra were taken on an automated DRON-4.0-07 diffractometer with CoK_α and CuK_α radiation sources. The recording was performed in the step scanning mode within the angle range of 20°–120° with a recording step of 0.1° and an exposure time of 4 s. Nanoindentation was performed with a three-sided Berkovich indenter on a Nano Indenter G200 nanohardness tester manufactured by Agilent Technologies (USA); the indentation depth was 200 nm. The tests were carried out on the sample matrix and inclusions. Figure 4 shows impressions from the indenter after tests on the matrix and inclusions of the $20SiC_{micro}$–$80Al_2O_3$ nanosample.[1]

At least ten imprints were made on each sample at a distance of 15 μm on inclusions and 25 μm from each other on the matrix to avoid the influence of neighboring imprints on the test results, and then the obtained data were averaged. To find the hardness and elastic modulus, the method of Oliver and Pharr [19] was used. A sample of fused quartz was tested before starting the tests of the samples, which serves as a hardness standard during nanoindentation, since it does not have a large-scale effect and deformation hardening of the surface during its mechanical processing. The obtained data for fused quartz ($E = 72$ GPa and $H = 9.2$ GPa) confirm that the instrument is reliably calibrated.

The microhardness and crack resistance values were determined by measuring the imprint diagonal and the length of the radial cracks obtained during indentation of a diamond indenter in the form of a four-sided pyramid with an angle of $\alpha = 136°$ near the tip (Vickers pyramid) on a NEXUS 4504 automatic microhardness tester. The load was $P = 10$ N, and the exposure time was 10 s.

The microhardness determined was determined using the following expression [20]:

$$H_V = \frac{kP}{(2a)^2}, \quad (1)$$

[1] Hereinafter, the composition of ceramics is given in wt %.

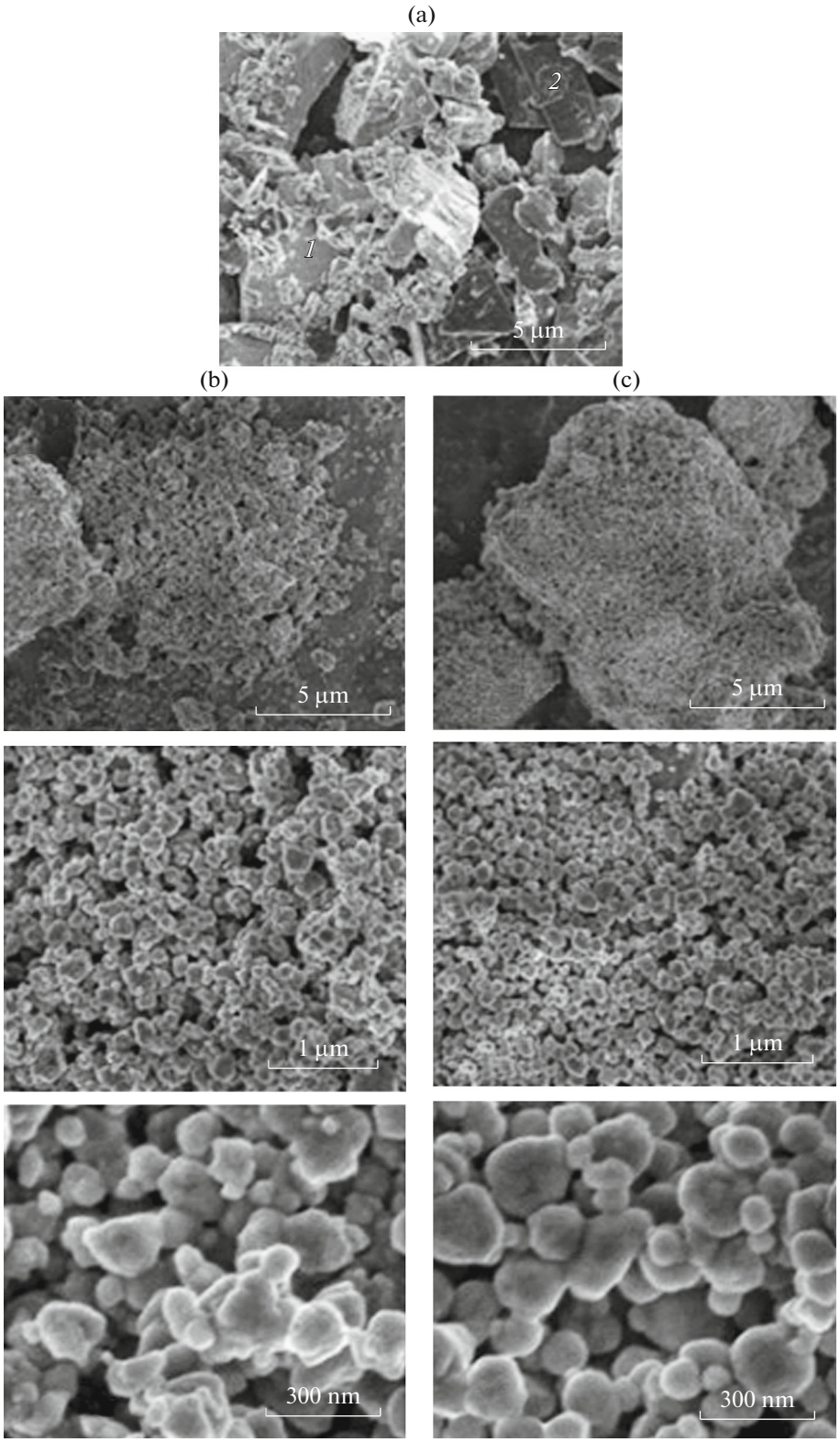

Fig. 1. Microstructures of (a) the initial SiC mixture, (b) the mixture after 90 min of mechanical activation, and (c) the SBC product.

where P is the load on the indenter, kg; $2a$ is the average value of the lengths of both diagonals of the imprint, μm; k is a coefficient that depends on the shape of the indenter (for the Vickers pyramid, k = 1.854).

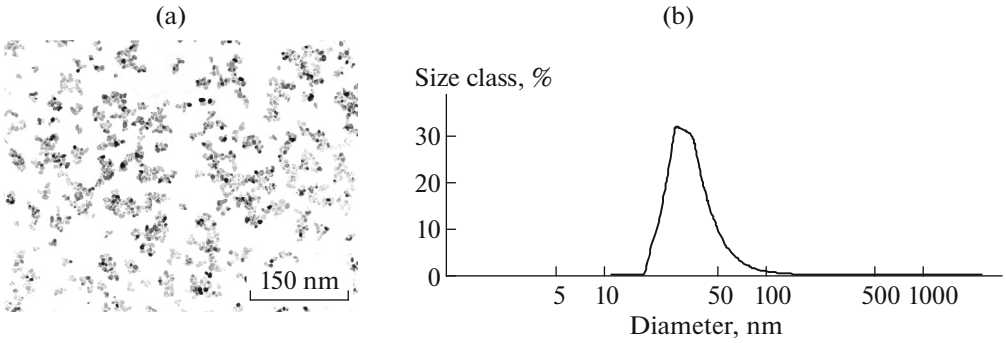

Fig. 2. Microphotograph of (a) ZrO_2 nanoparticles and their size distribution (b).

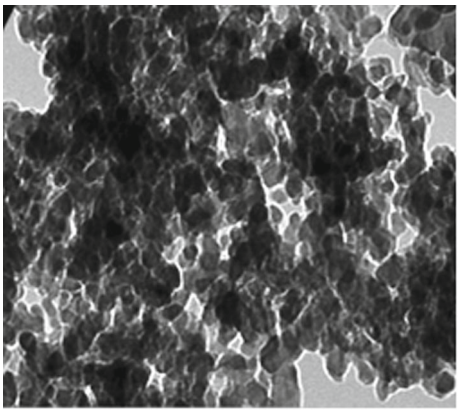

Fig. 3. Microphotograph of α-Al_2O_3 nanoparticles.

Fracture viscosity coefficient K_{Ic}, which characterizes the crack resistance of the sample, was determined by the following expression [21, 22]

$$K_{Ic} = \zeta\left(\frac{l}{a}\right)^{-0.5}\left(\frac{H_V}{EF}\right)^{-0.4}\frac{H_V a^{0.5}}{F}, \quad (2)$$

where ζ is a dimensionless constant (for ceramics, it has an average value of 0.016); E is the Young modulus, GPa; H_V is the hardness, GPa; F is a constant ($F \approx 3$); l is the length of the crack from the corner of the imprint of the Vickers pyramid, m; a is the semidiagonal of the imprint of the Vickers pyramid, m.

The following conditions were fulfilled during the calculation:

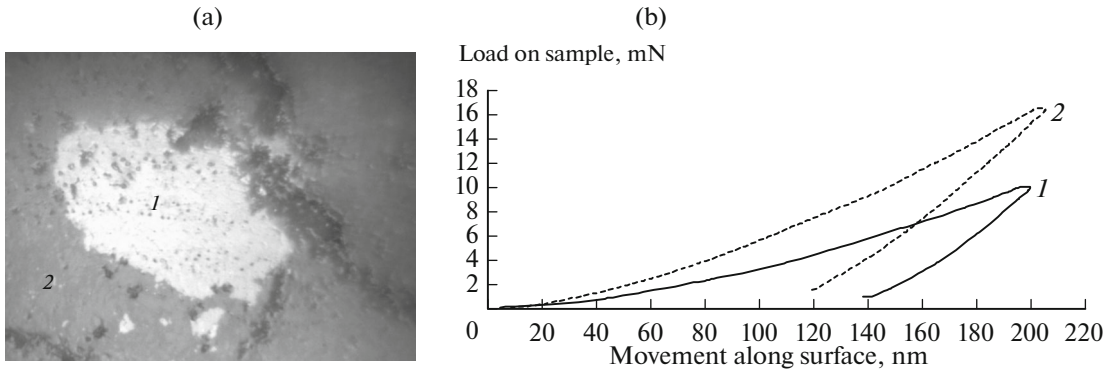

Fig. 4. Loading curves in (a) the matrix and (b) inclusions for $20SiC_{micro}$–$Al_2O_{3\ nano}$.

$$0.25 \le \frac{l}{a} \le 2.5. \quad (3)$$

The strength limit during bending of the sample under conditions of three-point bending was determined by the following expression [23]:

$$\sigma_{\text{flex}} = \frac{3PL}{2bh^2}, \quad (4)$$

where P is the force at the moment of dividing the sample into parts, N; L is the sample length, mm; b is the sample width, mm; h is the sample thickness in the direction parallel to the force applied to the sample, mm.

The heat conductivity was measured using the stationary heat flow method [24]. This method makes it possible to measure the temperature dependence of the heat conductivity in a wide temperature range. A rod whose length was several times larger than the cross size was cut from the finished compressed sample. The resulting rod was placed between the receiver and the heat source, due to which a longitudinal heat flow and a temperature gradient were created in it. The installation was comprised of a cryostat, i.e., a hermetically sealed cell with a sample placed in the container with liquid helium, which was immersed, in turn, in liquid nitrogen. To reduce heat losses, the air from the chamber was evacuated to a pressure of about 10^{-7} mm Hg. Inside the chamber, the sample under test was placed in the thermostat, to which a heat source (heater) and a differential copper–constantan thermocouple were attached. The temperature was measured with a platinum resistance thermometer. With small differences in the mounting of the sample in the cryostat, it was possible to measure not only the heat conductivity, but also other transport characteristics of the solid body, such as the thermal diffusivity and electrical conductivity.

Silicon carbide refers to compounds that have strong covalent bonds, which complicates mass transfer during sintering without the use of activating impurities and the application of external pressure [25]. To obtain dense SiC ceramics, the method of liquid phase sintering with use of oxide impurities is typically employed [26, 27]. The most important conditions of this method are a decrease in the temperature of the appearance of the liquid phase under the condition of its minimum viscosity and good wettability of the surface of silicon carbide particles [28]. High density indicators were obtained with an oxide impurity content of 10 wt %, and the maximum shrinkage of the samples was observed with an impurity content of 20 wt %.

RESULTS AND DISCUSSION

In the process of heating during electroconsolidation, the following reaction occurs between SiC and oxides:

$$SiC_{(solid)} + Al_2O_{3(solid)} \rightarrow SiO_{(gas)} + Al_2O_{3(gas)} + CO_{(gas)}. \quad (5)$$

Therefore, it is necessary to take into account the release of CO gases in the process of hot pressing; for this, it is necessary to hold the reaction in the temperature range of 800–1000°C for up to 10 min in order to release CO gases.

To form a liquid phase, Al_2O_3 and ZrO_2 powders were used as impurities, the mixture of which has a melting temperature of 1860°C and form a liquid phase when mixed in the ratio of 60 and 40 mol %, respectively [29, 30]. Figure 5 shows the structure of SiC ceramics with an admixture of aluminum oxide.

To determine the optimal content of the admixture of an aluminum oxide nanopowder, the composition with the same content of both components was first studied. The sintering temperature was empirically chosen based on the possibility of obtaining the densest samples. Figure 6 shows the phase diagram of the Al_2O_3–ZrO_2 system.

The maximum density was obtained with the silicon carbide, aluminum oxide, and zirconium oxide contents corresponding to the eutectic composition (Table 2).

A study of the physical and mechanical properties of SiC-based materials obtained by liquid-phase sintering with two activating impurities of aluminum oxide and zirconium dioxide nanopowders showed that the density in the case of sintering of the eutectic composition at a temperature of 1860 °C is almost 100%. With a different composition of the initial mixture and in the case of sintering at a temperature below 1860°C, incomplete wetting of the SiC surface by oxides occurs and, as a result, the density of the composite and the level of mechanical properties decrease (Fig. 7).

Samples of products based on SiC micropowders with an admixture of aluminum oxide nanopowders had the following maximum mechanical properties:

$$\sigma_{\text{flex}} = 560 \pm 10 \text{ MPa};$$

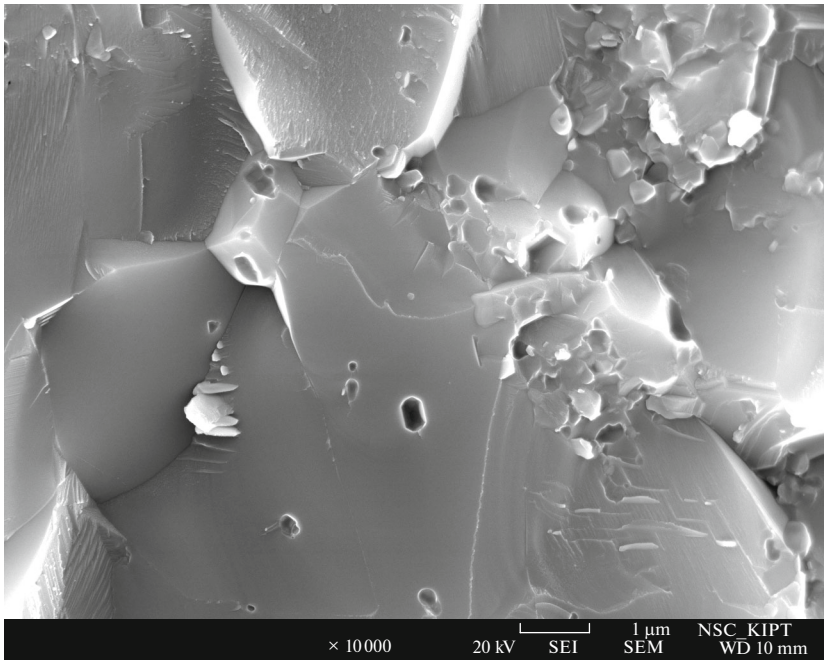

Fig. 5. Structure of hot-pressed SiC–50Al_2O_3 at a temperature of $T = 1600$°C, a pressure of 30 MPa, and a residing time of 3 min.

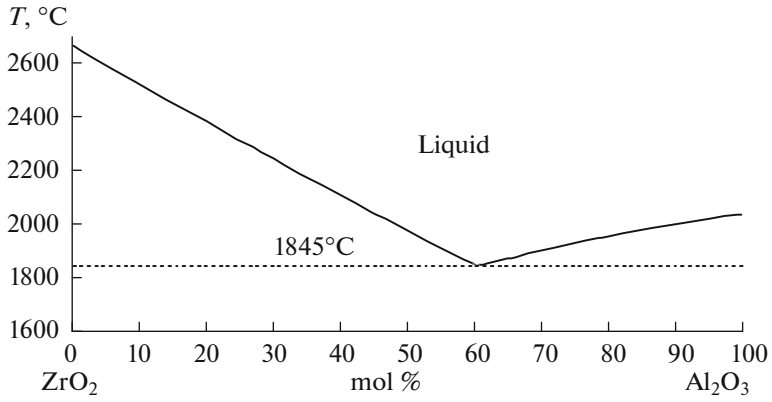

Fig. 6. Phase diagram of the Al_2O_3–ZrO_2 system.

$$H_V = 22.3 \pm 0.2 \text{ GPa};$$

$$K_{Ic} = 5.5 \pm 0.2 \text{ MPa m}^{1/2}.$$

The result of the X-ray phase analysis of one of the samples obtained from a mixture of starting powders (see sample 7 in Table 2) is shown in Fig. 8.

The composite material obtained using liquid-phase pressing (Fig. 7), has the following physical and mechanical properties:

— flexural strength limit 800–1000 MPa;

— crack resistance 6–8 MPa $m^{1/2}$;

— hardness 91–93 HRA;

— heat conductivity coefficient 30–35 W/(m K).

In fact, the mechanical strength of ceramics is determined by the physical and mechanical properties of the homogeneous eutectic medium–(silicon carbide micropowder + nanodispersed aluminum and zirconium oxides) system, which itself is a ceramic nanocomposite of the micro/nano type (Fig. 9). In this

Table 2. Density of initial mixtures with different compositions

No.	SiC, wt %	Al_2O_3, wt %	ZrO_2, wt %	T_{annel}, °C	ρ_{theor}, g/cm^3	ρ_{exp}, g/cm^3	ρ_{exp}/ρ_{theor}, %
1	50	50	–	1600	3.54	3	85
2	30	70	–	1500	3.68	2.83	77
3	10	90	–	1500	3.85	3.4	88
4	80	20	–	1600	3.34	2.1	63
5	60	40	–	1600	3.5	2.6	74
6	80	12	8	1860	3.4	3.4	100
7	80	20	–	1700	3.34	3.1	95
8	80	12	8	1700	3.4	3.2	96

case, the mechanism of destruction of the material changes fundamentally. The crack passes through a homogeneous eutectic medium, and the intercrystalline fracture actually turns into a transcrystalline fracture.

Moreover, the high strength of the interface with the matrix provides a substantial shielding stress and a sharp increase in both the strength and crack resistance when the dispersed phase is represented by a brittle material, the destruction of which occurs even in the event of a small opening of the crack.

Figure 10 shows the fractogram of the sample obtained on the basis of initial mixtures with an eutectic composition.

It should be noted that quite interesting results were obtained when the $Al_2O_{3\ nano}$–$20SiC_{micro}$ nanopowder was used as a basis of the composite material.

In this case, the nanohardness and elastic modulus of individual Al_2O_3 and SiC phases were investigated. The fairly high hardness and elastic modulus values allow us to assume that the resulting composite material will exhibit high wear resistance (Fig. 11, Table 3).

As can be seen from Fig. 11, agglomerates of aluminum oxide nanopowder are visible in points 2 and 3, which is a result of insufficiently good mixing of the original powders. Nanohardness and elastic modulus measurements of individual phases of the same sample show a large difference in the nanohardness and elastic modulus of the individual phases.

Fractograms and phase characteristics of silicon carbide (Fig. 12) and aluminum oxide (Fig. 13) are given for the $20SiC_{micro}$–$80Al_2O_{3\ nano}$ composite sintered at a temperature of 1700°C under a pressure of 30 MPa with an exposure time of 3 min.

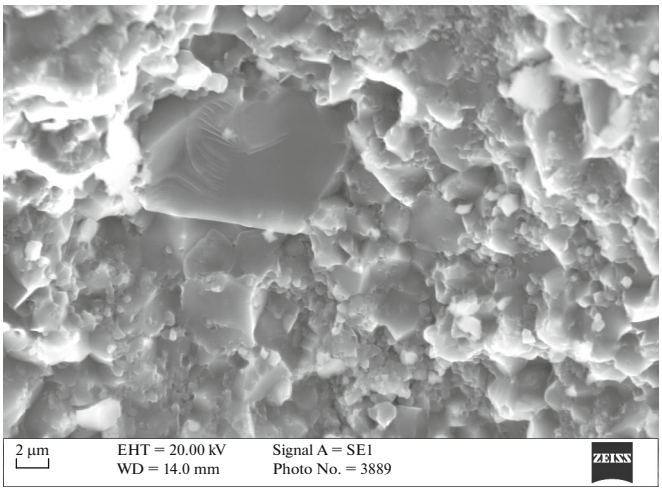

Fig. 7. Fractogram of the hot-pressed initial SiC–$12ZrO_2$–$8Al_2O_3$ mixture at a temperature of 1700°C, a pressure of 30 MPa, and a residing time of 3 min.

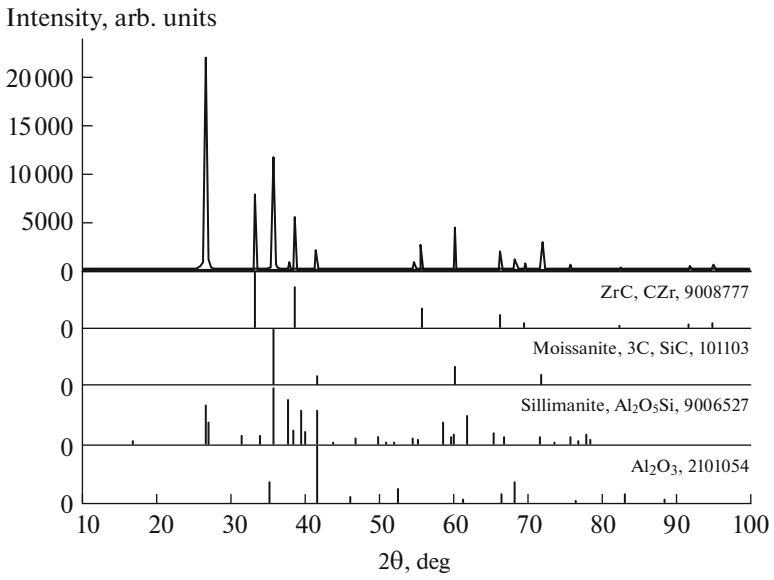

Fig. 8. X-ray diffractograms of SiC–12ZrO_2–8Al_2O_3 ceramics sintered at a temperature of 1860°C, a pressure of 30 MPa, and a residing time of 3 min.

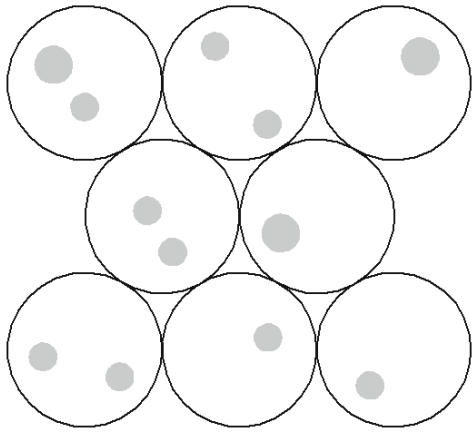

Fig. 9. Structure of the material of the micro/nano type.

Thus, it can be assumed that the combination of a matrix of micropowder grains and admixtures of nanopowders of refractory oxides in the initial mixtures allows one to obtain composite materials with high hardness, crack resistance, and elastic modulus charcateristics. However, it is necessary to investigate how heating to temperatures above 1000°C will affect the mechanical properties of composite materials

Table 3. Density of initial mixtures with different compositions

Point	C	O	Al	Si	Total, %
1	–	38.86	60.45	0.69	100.00
2	–	53.27	46.73	–	100.00
3	–	53.61	46.39	–	100.00
4	6.72	44.97	40.80	7.51	100.00
5	6.18	51.22	38.06	4.54	100.00
6	11.09	41.18	29.35	18.38	100.00

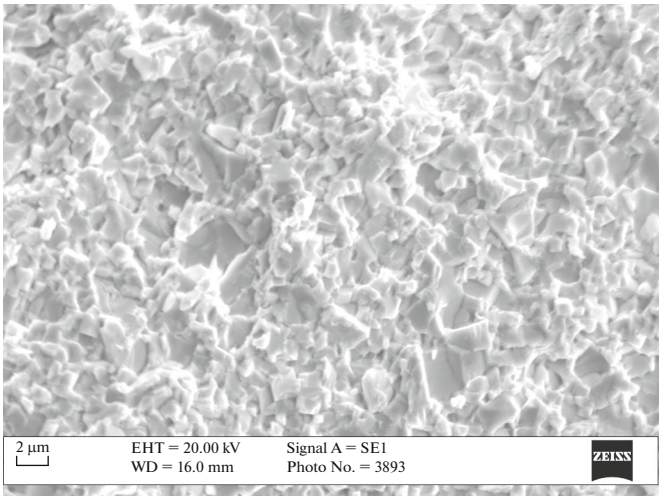

Fig. 10. Fractogram of the hot-pressed composite from the initial 80SiC + 20(Al_2O_3 + ZrO_2) mixture at a temperature of 1860°C, a pressure of 30 MPa, and a residing time of 3 min.

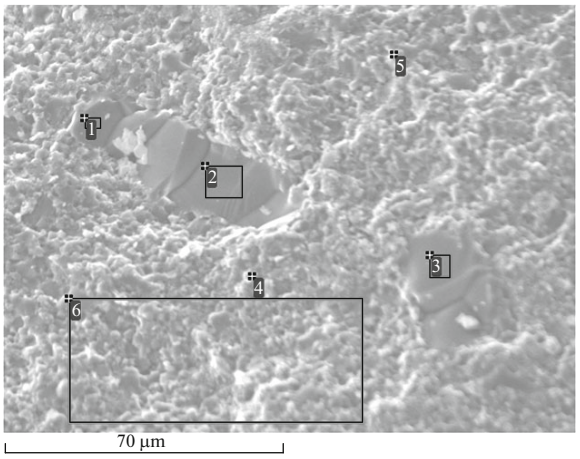

Fig. 11. Spectral analysis of the composite material obtained from the initial $Al_2O_{3\ nano}$–20SiC mixture by hot pressing in vacuum at a temperature of 1600°C, a pressure of 30 MPa, and a residing time of 3 min.

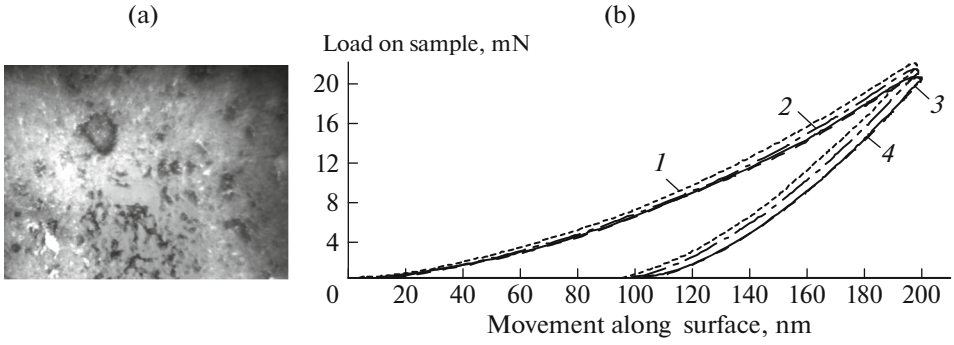

Fig. 12. (a) Fractogram and (b) characteristics of the silicon carbide phase with a nanohardness of $E = 446 \pm 15$ GPa and an elastic modulus of $H = 30.6 \pm 2$ GPa.

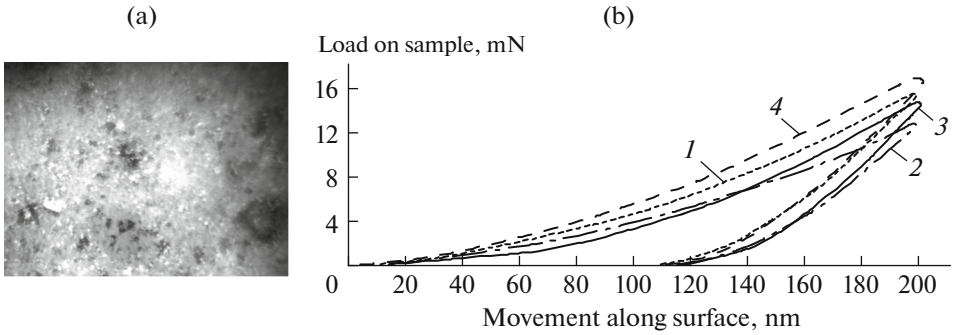

Fig. 13. (a) Fractogram and (b) characteristics of the aluminum oxide phase with a nanohardness of $E = 348 \pm 29$ GPa and an elastic modulus of $H = 19.5 \pm 3$ GPa.

based on silicon carbide. This is very important if the material is intended to be used as a thermal abrasive nozzle or under other heavy-duty conditions.

CONCLUSIONS

The samples prepared using the 80SiC + 20(Al_2O_3 + ZrO_2) eutectic compositions have the highest hardness and crack resistance characteristics. It was determined that the optimal modes of sintering of eutectic composition mixtures are achieved at a temperature of 1860°C, a pressure of 30 MPa, and an exposure time of 3 min. Samples obtained from mixtures of the $Al_2O_{3\ nano}$–SiC_{micro} system by hot pressing at a temperature of 1600°C also have high values of the hardness and elastic modulus. High values of the hardness and elastic modulus cause high wear resistance of the obtained composite material, which will allow it to be used as a material for ceramic inserts of abrasive jet nozzles with a straight channel.

The performed experiments make it possible to state that a high solubility of the solid substance in the liquid phase is not required for high-quality compaction in the process of liquid-phase sintering. On the contrary, it should be avoided, since a high solubility can lead to deformation of the material and its subsequent destruction. Moreover, there is a problem of uniform distribution of modifiers over the surface of their particles in the technology of ceramics synthesis in the case of using nanodisperse powders as starting materials.

To solve this problem and improve the processes of controlling the structure of materials based on silicon carbide, which contain impurities of eutectic compositions, it is advisable to use the method of heterophase chemical deposition directly on silicon carbide particles. This will make it possible to obtain a more perfect microstructure, to effectively carry out the high-temperature compaction process, and to reduce the probability of the reaction of SiC with the melt, which leads to the formation of gaseous products.

CONFLICT OF INTEREST

The authors declare that they have no conflicts of interest.

REFERENCES

1. Huang, Q.-W. and Zhu, L.-H., High-temperature strength and toughness behaviors for reaction-bonded SiC ceramics below 1400°C, *Mater. Lett.*, 2005, vol. 59, nos. 14–15, pp. 1732–1735.
2. Gevorkyan, E.S., Rucki, M., Kagramanyan, A.A., and Nerubatskiy, V.P., Composite material for instrumental applications based on micro powder Al_2O_3 with additives nano-powder SiC, *Int. J. Refract. Met. Hard Mater.*, 2019, vol. 82, pp. 336–339.
3. Arellano-López, A.R., Martínez-Fernández, J., González, P., Domínguez, C., Fernández-Quero, V., and Singh, M., Biomorphic SiC: A new engineering ceramic material, *Int. J. Appl. Ceram. Technol.*, 2005, vol. 1, no. 1, pp. 56–67.
4. Gevorkyan, E., Mamalis, A., Vovk, R., Semiatkowski, Z., Morozow, D., Nerubatskyi, V., and Morozova, O., Special features of manufacturing cutting inserts from nanocomposite material Al_2O_3–SiC, *J. Instrum.*, 2021, vol. 16, no. 10, P10015.
5. Yaşar, Z.A. and Haber, R.A., Effect of carbon addition and mixture method on the microstructure and mechanical properties of silicon carbide, *Materials*, 2020, vol. 13, no. 17, 3768.

6. Biscay, N., Henry, L., Adschiri, T., Yoshimura, M., and Aymonier, C., Behavior of silicon carbide materials under dry to hydrothermal conditions, *Nanomaterials*, 2021, vol. 11, 1351.
7. Bardakhanov, S.P., Goverdovskiy, V.N., Lee, C.-M., Lee, O.C., and Lygdenov, V.T., Analysis and alternate selection of nanopowder modifiers to improve a special protective coating system, *Adv. Mater. Sci. Eng.*, 2017, vol. 2017, 2397238.
8. Gevorkyan, E.S., Nerubatskyi, V.P., Chyshkala, V.O., and Morozova, O.M., Aluminum oxide nanopowders sintering at hot pressing using direct current, *Mod. Sci. Res.*, 2020, no. 14 (1), pp. 12–18.
9. Gevorkyan, E., Nerubatskyi, V., Chyshkala, V., and Morozova, O., Revealing specific features of structure formation in composites based on nanopowders of synthesized zirconium dioxide, *East.-Eur. J. Enterp. Technol.*, 2021, vol. 5, no. 12 (113), pp. 6–19.
10. Shukla, M., Ghosh, S., Dandapat, N., Mandal, A., and Balla, V., Comparative study on conventional sintering with microwave sintering and vacuum sintering of Y_2O_3–Al_2O_3–ZrO_2 ceramics, *J. Mater. Sci. Chem. Eng.*, 2016, vol. 4, pp. 71–78.
11. Borrell, A. and Dolores, M., Advanced ceramic materials sintered by microwave technology, in *Sintering Technology—Method and Application*, Intech, 2018.
12. Gevorkyan, E., Rucki, M., Krzysiak, Z., Chishkala, V., Zurowski, W., Kucharczyk, W., Barsamyan, V., Nerubatskyi, V., Mazur, T., Morozow, D., Siemiątkowski, Z., and Caban, J., Analysis of the electroconsolidation process of fine-dispersed structures out of hot pressed Al_2O_3–WC nanopowders, *Materials*, 2021, vol. 14, no. 21, 6503.
13. Gevorkyan, E., Rucki, M., Sałaciński, T., Siemiątkowski, Z., Nerubatskyi, V., Kucharczyk, W., Chrzanowski, Ja., Gutsalenko, Yu., and Nejman, M., Feasibility of cobalt-free nanostructured WC cutting inserts for machining of a TiC/Fe composite, *Materials*, 2021, vol. 14, no. 12, 3432.
14. Goldberger, W.M. and Merkle, B.D., Electroconsolidation offers fast, low-cost densification, *Met. Powder Rep.*, 2001, vol. 56, no. 2, pp. 30–33.
15. Agrawal, D., Microwave sintering of ceramics, composites and metallic materials, and melting of glasses, *Trans. Indian Ceram. Soc.*, 2006, vol. 65, no. 3, pp. 129–144.
16. Mukasyan, A.S., Lin, Ya-Ch., Rogachev, A.S., and Moskovskikh, D.O., Direct combustion synthesis of silicon carbide nanopowder from the elements, *J. Am. Ceram. Soc.*, 2013, vol. 96, no. 1, pp. 111–117.
17. McCall, J.L., Scanning electron microscopy for microstructural analysis, in *Microstructural Analysis*, McCall, J.L. and Mueller, W.M., Eds., Boston: Springer, 1973, pp. 93–124.
18. Gevorkyan, E., Nerubatskyi, V., Chyshkala, V., Gutsalenko, Y., and Morozova, O., Determining the influence of ultra-dispersed aluminum nitride impurities on the structure and physical-mechanical properties of tool ceramics, *East.-Eur. J. Enterp. Technol.*, 2021, vol. 6, no. 12 (114), pp. 40–52.
19. Oliver, W.C. and Pharr, G.M., An improved technique for determining hardness and elastic modulus using load and displacement sensing indentation experiments, *J. Mater. Res.*, 1992, vol. 7, pp. 1564–1583.
20. Rad'ko, I.P. and Markhon', M.V., Peculiarities of the study of the adhesion strength of composite contact materials with worn parts of electrical equipment, *Tekh. Energ.*, 2016, no. 252, pp. 176–185.
21. *GOST* (State Standard) *25.506-85*: *Calculations and Strength Tests. Methods of Mechanical Testing of Metals. Determination of Characteristics of Crack Resistance (Fracture Toughness) under Static Loading*, Moscow: Izd. Standartov, 1985.
22. Quinn, G.D., Fracture toughness of ceramics by the vickers indentation crack length method: A critical review, in *Mechanical Properties and Performance of Engineering Ceramics II: Ceramic Engineering and Science Proceedings*, 2006, vol. 27, pp. 45–62.
23. Podrezov, Yu.M., Varbilo, D.G., Danilenko, V.I., Tsiganenko, N.I., Shurigin, B.V., and Romanko, P.M., *Elektron. Mikrosk. Prochn. Mater., Ser: Fiz. Materialoved. Strukt. Svoistva Mater.,* 2018, vol. 24, pp. 35–46.
24. Wilkinson, D.S. and Ashby, M.F., Pressure sintering by powder law creep, *Acta Metall.,* 1975, vol. 23, no. 11, pp. 1277–1285.
25. Ageev, O.A., Belyaev, A.E., Boltovets, N.S., Kiselev, V.S., and Konakova, R.V., *Karbid kremniya: tekhnologiya, svoistva, primenenie* (Silicon Carbide: Technology, Properties, Application), Belyaev, A.E. and Konakova, R.V., Eds., Kharkiv: ISMA, 2010.
26. Sigl, L.S., Thermal conductivity of liquid phase sintered silicon carbide, *J. Eur. Ceram. Soc.*, 2003, vol. 23, no. 7, pp. 1115–1122.
27. Vorotilo, S., Patsera, E., Shvindina, N., Rupasov, S., and Levashov, E., Effect of in situ grown SiC nanowires on the pressureless sintering of heterophase ceramics $TaSi_2$–TaC–SiC, *Materials*, 2020, vol. 13, no. 15, 3394.
28. Gomez, E., Echeberria, J., Iturriza, I., and Castro, F.J., Liquid phase sintering of SiC with additions of Y_2O_3, Al_2O_3 and SiO_2, *J. Eur. Ceram. Soc.*, 2004, vol. 24, no. 9, pp. 2895–2903.
29. Jerebtsov, D.A., Mikhailov, G.G., and Sverdina, S.V., Phase diagram of the system: Al_2O_3–ZrO_2, *Ceram. Int.*, 2000, vol. 26, no. 8, pp. 821–823.
30. Gevorkyan, E., Nerubatskyi, V., Gutsalenko, Yu., Melnik, O., and Voloshyna, L., Examination of patterns in obtaining porous structures from submicron aluminum oxide powder and its mixtures, *East.-Eur. J. Enterp. Technol.*, 2020, vol. 6, no. 6 (108), pp. 41–49.

Translated by O. Kadkin